Emerging Techniques in Cardiac Magnetic Resonance Imaging

Guo, Rui; Weingärtner, Sebastian; Šiurytė, Paulina; T. Stoeck, Christian; Füetterer, Maximilian; E. Campbell-Washburn, Adrienne; Suinesiaputra, Avan; Jerosch-Herold, Michael; Nezafat, Reza

DOI
10.1002/jmri.27848

Publication date
2021

Document Version
Accepted author manuscript

Published in
Journal of Magnetic Resonance Imaging

Citation (APA)
Guo, R., Weingärtner, S., Šiurytė, P., T. Stoeck, C., Füetterer, M., E. Campbell-Washburn, A., Suinesiaputra, A., Jerosch-Herold, M., & Nezafat, R. (2021). Emerging Techniques in Cardiac Magnetic Resonance Imaging. *Journal of Magnetic Resonance Imaging*, *55*(4), 1043-1059. https://doi.org/10.1002/jmri.27848

Emerging Techniques in Cardiac Magnetic Resonance Imaging

Rui Guo, PhD,[1] Sebastian Weingärtner, PhD,[2] Paulina Šiurytė, MSc,[2] Christian T. Stoeck, PhD,[3] Maximilian Füetterer, PhD,[3] Adrienne E. Campbell-Washburn, PhD,[4] Avan Suinesiaputra, PhD,[5] Michael Jerosch-Herold, PhD,[6] and Reza Nezafat, PhD[1*]

Cardiovascular disease is the leading cause of death and a significant contributor of health care costs. Noninvasive imaging plays an essential role in the management of patients with cardiovascular disease. Cardiac magnetic resonance (MR) can noninvasively assess heart and vascular abnormalities, including biventricular structure/function, blood hemodynamics, myocardial tissue composition, microstructure, perfusion, metabolism, coronary microvascular function, and aortic distensibility/stiffness. Its ability to characterize myocardial tissue composition is unique among alternative imaging modalities in cardiovascular disease. Significant growth in cardiac MR utilization, particularly in Europe in the last decade, has laid the necessary clinical groundwork to position cardiac MR as an important imaging modality in the workup of patients with cardiovascular disease. Although lack of availability, limited training, physician hesitation, and reimbursement issues have hampered widespread clinical adoption of cardiac MR in the United States, growing clinical evidence will ultimately overcome these challenges. Advances in cardiac MR techniques, particularly faster image acquisition, quantitative myocardial tissue characterization, and image analysis have been critical to its growth. In this review article, we discuss recent advances in established and emerging cardiac MR techniques that are expected to strengthen its capability in managing patients with cardiovascular disease.
Level of Evidence: 5
Technical Efficacy: Stage 1

J. MAGN. RESON. IMAGING 2021.

Cardiac magnetic resonance (MR) is a powerful imaging modality in the evaluation of patients with cardiovascular disease. Over the past two decades, there has been significant growth in both research and clinical applications of cardiac MR. In addition to cardiac function and structural measures, cardiac MR provides deep phenotyping of myocardial tissue composition to assess myocardial fibrosis, edema, perfusion, and microstructure. This review article will highlight recent advances in cardiac MR, focusing on technical developments in data acquisition and analysis.

Myocardial Tissue Characterization

Cardiac MR can noninvasively assess heart and vascular abnormalities, including biventricular structure/function, blood hemodynamics, myocardial tissue composition, microstructure, perfusion, metabolism, coronary microvascular function, and aortic distensibility/stiffness (Fig. 1). One of the main advantages of cardiac MR over other cardiac imaging modalities is its ability to noninvasively characterize myocardial tissue composition.

Evaluation of myocardial viability with late gadolinium enhancement (LGE) is the most common indication for a cardiac MR examination. In the LGE sequence, T_1-weighted images are collected after an inversion pulse. Due to differences in T_1 times between healthy and scarred myocardium, the scar appears bright. However, use of an incorrect inversion time may result in artifactual enhancement.

View this article online at wileyonlinelibrary.com. DOI: 10.1002/jmri.27848

Received Apr 8, 2021, Accepted for publication Jul 9, 2021.

*Address reprint requests to: R.N., 330 Brookline Avenue, Boston, MA 02215, USA. E-mail: rnezafat@bidmc.harvard.edu

From the [1]Department of Medicine (Cardiovascular Division), Beth Israel Deaconess Medical Center and Harvard Medical School, Boston, Massachusetts, USA; [2]Department of Imaging Physics, Magnetic Resonance Systems Lab, Delft University of Technology, Delft, The Netherlands; [3]Institute for Biomedical Engineering, University and ETH Zurich, Zurich, Switzerland; [4]Cardiovascular Branch, Division of Intramural Research, National Heart, Lung, and Blood Institute, National Institutes of Health, Bethesda, Maryland, USA; [5]Faculty of Engineering and Physical Sciences, University of Leeds, Leeds, UK; and [6]Department of Radiology, Brigham and Women's Hospital and Harvard Medical School, Boston, Massachusetts, USA

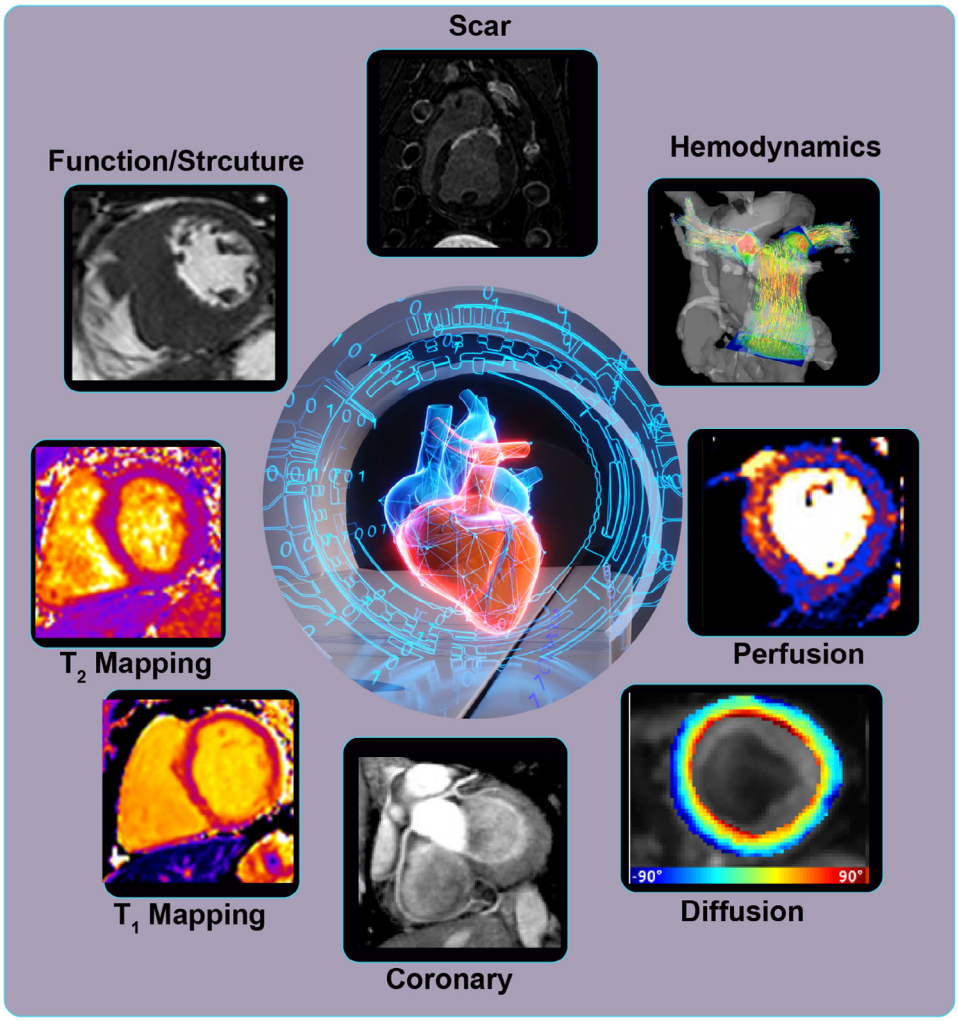

FIGURE 1: Cardiac MR imaging provides a comprehensive assessment of the structure, function, perfusion, viability, hemodynamics, microstructure, and myocardial mapping via T_1, T_2, and T_2^*. The imaging protocol typically includes basic function, structure, flow, and the remaining necessary sequences are tailored based on the patient indication with a typical scan time of 45–60 minutes.

Phase-sensitive inversion recovery (PSIR) was introduced to preserve information about longitudinal magnetization polarity.[1] To further improve blood-scar contrast for better visualization of sub-endocardial scars, dark blood LGE (DB-LGE) sequences were developed.[2–6] In DB-LGE, additional contrast mechanisms such as T_2 preparation or magnetization transfer (MT) are exploited to enhance blood-scar contrast. In the first approach, T_2 preparation is used in addition to inversion pulse, with sequence timings configured to suppress the signal from both the blood and normal myocardium.[2,3] Similarly, a combination of MT off-resonance excitations and inversion recovery achieves dark-blood contrast.[4] Gray-blood LGE has also been introduced to retain some blood pool signal, with the potential for improved anatomical assessment.[5] These specialized sequences require additional steps to optimize the new imaging parameters and achieve blood signal suppression. A PSIR-specific inversion time optimization has also been used to achieve DB-LGE without additional preparation sequences.[6] LGE is commonly acquired using a series of two-dimensional (2D) slices. However, recent advances in accelerated imaging and respiratory motion correction have enabled whole heart three-dimensional (3D) LGE, allowing higher spatial resolution and whole heart coverage, albeit with significantly longer scan times.[7] Advanced accelerating techniques such as compressed sensing (CS)[7,8] and, most recently, deep learning (DL)-based reconstructions[9] can be used to further reduce the scan time.

LGE imaging requires the administration of a gadolinium-based contrast agent (GBCA). Indeed, the majority of cardiac MR examinations are performed with GBCA. There are currently two classes of GBCA available for cardiac MR examinations: linear and macrocyclic, each with varying properties and safety profiles. With emerging data on the superior safety of macrocyclic GBCA, cardiac MR examinations are mainly performed using a macrocyclic agent with a favorable safety profile.[10] Intravascular "blood-pool" contrast agents (eg, gadofosveset trisodium (Ablavar™)) have been previously used for vascular imaging and are highly popular

in pediatric cardiac imaging. However, they are no longer clinically available. Therefore, macrocyclic GBCA agents are currently the most widely used agents in cardiac MR.

In addition to myocardial viability, cardiac MR can assess the presence of diffuse interstitial fibrosis via T_1 and extracellular volume mappings, edema via T_2 mapping, and iron via T^*_2 mappings.[11] Numerous techniques have been proposed to perform T_1 mapping of the heart.[12] Most of these techniques are based on a T_1 sensitizing preparation, such as inversion or saturation pulse combined with a snapshot imaging readout, each with a distinct profile of advantages and disadvantages. An overview of the typical components of cardiac mapping sequences is provided in Fig. 2.

Modified Look-Locker Imaging (MOLLI)[13] is the only commercially available cardiac T_1 mapping sequence. Myocardial T_1 mapping with MOLLI is collected during a single breath-hold per slice with coverage of one to three slices. The analysis involves the manual drawing of the region of interest to delineate the myocardial signal for calculating global and regional T_1 values. A septal T_1 measurement is the most reproducible approach for quantification of global diffuse fibrosis in T_1 mapping. Saturation recovery-based T_1 mapping sequences (eg, SASHA[14] and SAPPHIRE[15]) are alternatives to inversion recovery-based sequences with improved accuracy, albeit reduced precision compared to MOLLI.[16] Despite the potential of alternative existing T_1 sequences to overcome several MOLLI confounders such as T_2 sensitivity, these sequences are only available for research purposes and not offered as a product by any magnetic resonance imaging (MRI) vendor. To improve patient comfort, free-breathing T_1 mapping, primarily based on the diaphragmatic navigator, has also been implemented.

T_2^* mapping is commonly achieved using multigradient echo readouts with variable echo times. Most modern techniques use dark blood contrast, acquired in the late diastole phase, where a double inversion recovery pulse is employed to null the blood signal and alleviate partial voluming effects.[17] A free-breathing alternative for T_2^* mapping was proposed, using single-shot imaging with multiple repetitions and motion correction in postprocessing.[18] T_2 mapping is commonly based on T_2 magnetization preparation modules combined with single-shot image readouts.[19,20] Rest periods are inserted between different acquisitions, allowing for signal recovery. Alternatively, saturation preparation avoids rest periods at the cost of reduced signal-to-noise ratio (SNR).[21] A two- or three-parameter fit model can be used for estimating T_2 values from T_2-weighted images.[22] Alternative sequence designs based on gradient- and spin-echo readout have also been proposed, potentially allowing gains in acquisition efficiency.[23] Finally, several free-breathing T_2 sequences emerged for multislice 2D/3D acquisitions with higher spatial coverage and spatial resolution.[21,24–26]

There have been recent advances in multiparametric mapping to simultaneously measure different tissue contrasts to reduce overall scan time and simplify the examination. Joint T_1 and T_2 mapping has been proposed, by combining

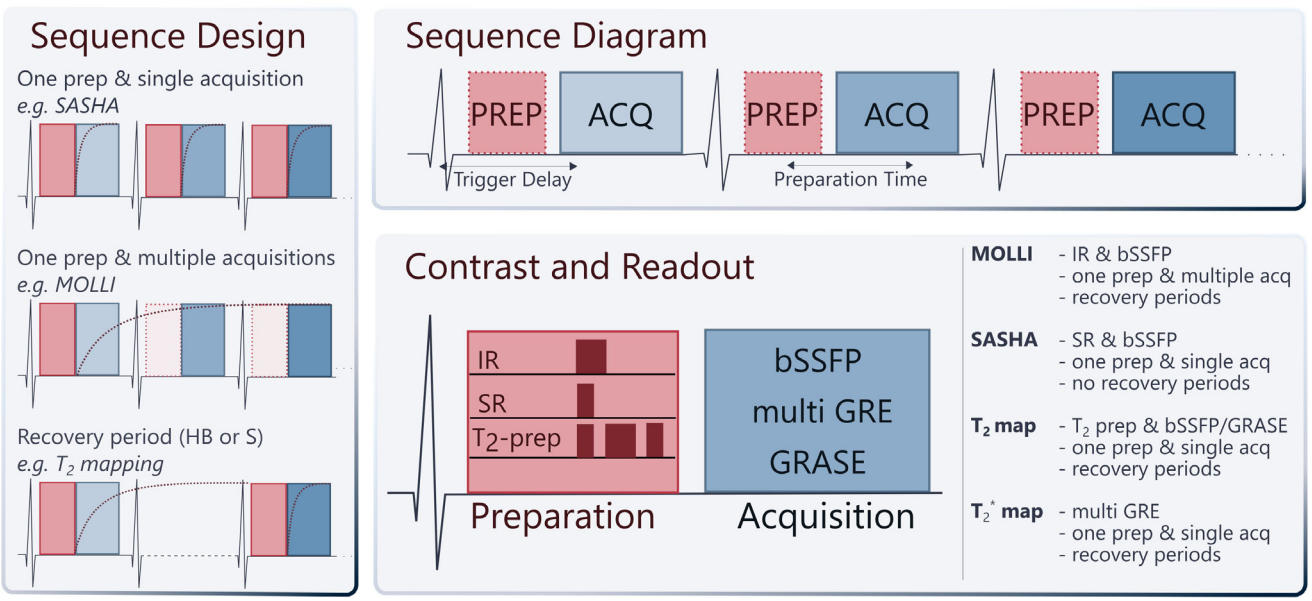

FIGURE 2: Commonly used myocardial tissue mapping sequences for evaluation of T_1, T_2, and T_2^*. The overall sequence design (left) describes ways of arranging preparation/acquisition blocks throughout the sequence duration and shows a schematic of the magnetization recovery curve (red dashed line). HB (heartbeats) and S (seconds) have been used as a unit for the recovery period. The sequence diagram (top right) depicts the layout of preparation and acquisition modules relative to the ECG. Dashed borders indicate that the preparation blocks may be left out depending on the sequence design. The contrast and readout (bottom right) list common choices for these building blocks. Each mapping sequence has a unique combination of the sequence design, trigger/preparation delay, preparation, and acquisition block.

T_1 sensitizing sequence elements, such as IR or SR pulses, with a T_2 preparation.[27–30] Cardiac MR fingerprinting (MRF) enables joint parameter mapping by unconventionally sampling with a very high temporal resolution and highly undersampled spiral readout.[31] A combination of preparation modules is used to sensitize the magnetization in cardiac MRF. Voxel-wise maps are then obtained by matching the signal evolution to precalculated dictionaries instead of conventional curve fitting. Multitasking is a new framework for multiparameter imaging of dynamic processes, in which signal dimensions such as T_1 and T_2 contrast or physiological motion are partially sampled, and low-rank tensor reconstructions are used to compensate for missing information.[32] Despite the potential of MRF and multitasking as promising free-running tissue characterization sequences, there are still numerous challenges, including lengthy reconstruction time, sensitivity to field inhomogeneity, and other imaging confounders that warrant further investigation prior to clinical adoption.

In addition to classical relaxometry parameters like T_1, T_2, T_2^*, other cardiac MRI markers for myocardial tissue characterization are emerging. Longitudinal relaxation in the rotating frame ($T_{1\rho}$) probes the molecular environment at intermediate frequencies below the Larmor frequency and is promising for detection of myocardial fibrosis.[33] MT, a well-established contrast mechanism for visualizing signals from bound pool protons in macromolecules, has been used for the assessment of myocardial fibrosis. Chemical exchange saturation transfer, based on proton exchange between free water and solute protons in metabolites like creatine, can also assess the metabolic activity and aid detection of infarcted tissue.[34] The sensitivity of these sequences to field inhomogeneity and cardiac motion remain major challenges. In addition, there is currently insufficient evidence to demonstrate the added value of acquisition of these newer contrasts compared to other established and widely available sequences for myocardial tissue characterization.

Myocardial Microstructures Imaging

Microstructural imaging plays a key role when linking myocardial function and structure and has gained significant momentum when investigating cardiac pathologies (Fig. 3). Diffusion-weighted/diffusion tensor imaging (DTI) has become an excellent tool to explore scalar-valued and directional information from the myocardial microstructure. Application to the heart has been challenging due to cardiac motion resulting in signal dropouts during imaging.[35] The development of motion compensation strategies, such as STimulated Echo Acquisition Mode (STEAM)[36] or specially designed second-order motion-compensated gradient waveforms[37,38] and dedicated postprocessing, have made diffusion-weighted and diffusion tensor cardiac MR possible.

Among all diffusion-related parameters, mean diffusivity (MD) is the simplest to derive. It relates to the distance water molecules can travel and, consequently, restrictions such as cell membranes. MD is typically computed from three orthogonally encoded diffusion-weighted images and an unweighted reference image, resulting in four required images. More recently, tensor-valued diffusion encoding has been proposed for DW-MRI only, requiring one diffusion-weighted and one reference image.[39] This approach unifies sampling and the three orthogonal directions in one acquisition, bringing DW-MRI a step closer to clinical application. The clinical potential of DW-/DT-MRI has been highlighted in recent studies examining the alteration in microstructure in various cardiac pathologies.

When the complete diffusion tensor is reconstructed, the degree of anisotropy of the underlying structure can be assessed using fractional anisotropy. Additionally, principal orientations of diffusion are derived by the computation of the diffusion tensor eigenvectors. Of particular interest is the direction of the first eigenvector aligned with the predominant myocyte orientation and the third eigenvector being perpendicular to myocyte bundles referred to as sheetlets.[40] Myocyte aggregate orientations in space are commonly characterized by the corresponding eigenvectors' angulation concerning a reference orientation.

Application of in vivo cardiac DTI imaging is growing. Current studies have mainly focused on identification of changes in DT cardiac MR-derived parameters in pathologies and comparison to conventional imaging methods. Khalique et al[41] showed abnormal systolic E2A and sheetlet mobility in recovered DCM patients indicating enduring microstructural alteration despite recovered left ventricular size and function. Gotschy et al[42] presented elevated transmural helix variation as a response to pressure overload due to aortic valve stenosis. Within 6 months of intervention, the cardiomyocyte aggregate orientation normalized with respect to the control cohort, illustrating the dynamic response of the myocardium to increased afterload. Consequently, investigating cardiac microstructure may help quantify cardiac burden at an early stage of disease. DT-MRI can also provide additional insights into the inner relationship between myocardial microstructure and function. Rodriguez et al[43] demonstrated a dominant contribution of sheetlet shear stain to radial thickening of the myocardium by combining DT-MRI and strain imaging. More recently, the concept of fiber strain has been investigated[44] and corresponding imaging and postprocessing have been engineered to ensure the feasibility of clinical application.[45] Despite recent advances toward clinical application, further development is needed to overcome low spatial resolution, insufficient ventricular coverage, and artifacts. DW-MRI, as well as DT-MRI, is an indirect measure of microstructure using diffusing water molecules as probing agents of their surroundings. Accordingly, pixel signal intensity reflects

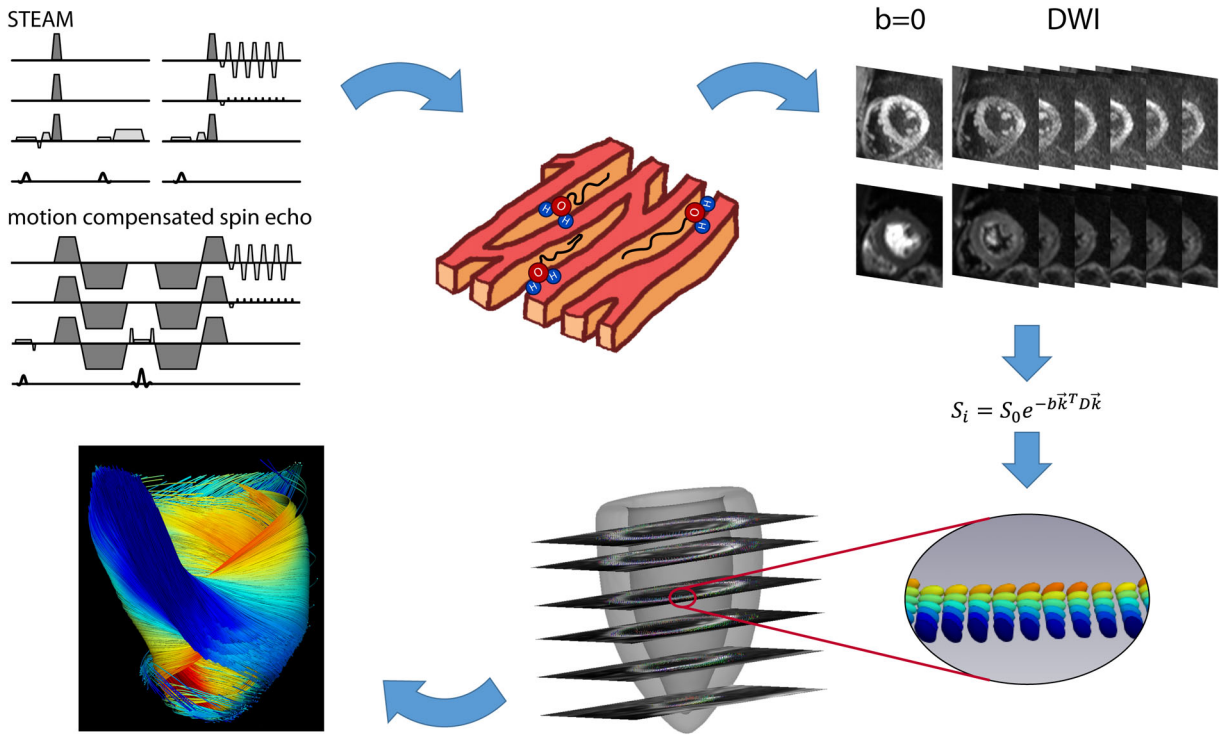

FIGURE 3: Cardiac diffusion imaging: Diffusion-weighted imaging using stimulated echo acquisition mode (STEAM) or motion-compensated spin-echo sequences senses the diffusivity of water molecules within the myocardium. To this end, diffusion sensitizing gradients are incorporated into imaging sequences (dark gray shaded areas). With the acquisition of one unweighted ($b = 0$) and at least six diffusion-weighted images (DWI), the diffusion tensor (D) can be computed. The principal eigenvector of the diffusion tensor is aligned with the average myocyte orientation within a voxel, and fiber tracking can consequently be performed to visualize the dominant double-helical myocyte alignment.

the average behavior of all water molecules diffusing within the voxel.

In addition to microstructural imaging, intravoxel incoherent motion imaging to assess myocardial perfusion has gained attention. The principle assumes quasi-random displacement of blood within the capillaries, similar to diffusing water molecules. It has been shown that the sensitivity of cardiac diffusion-weighted sequences to perfusion is strongly dependent on the sequence type and degree of motion compensation used.[46] With increased motion compensation and short mixing times, reduced sensitivity to perfusion has been reported, favoring STEAM imaging. Factors such as low intrinsic SNR of STEAM sequences, low sensitivity to perfusion of motion-compensated gradient waveforms used in spin-echo sequences, and required fitting of two exponential functions render intravoxel incoherent motion (IVIM) particularly challenging.

Cardiac DTI remains a research tool and can only be performed in specialized centers with access to home-grown sequences and analysis software. Currently, there is no standardized sequence accepted by the cardiac DTI community that can be used. Lack of access to software tools for deriving various parameters available in cardiac DTI images also poses a limitation. Further consensus statements and standardized sequences offered by vendors are needed to make this sequence available to nonexpert centers.

Myocardial Perfusion

Dynamic imaging of the heart during the first pass of a contrast bolus has been a long-standing focus in cardiac MRI and continues to push technical boundaries. The technique, also known as "first-pass perfusion imaging," is applied to a relatively wide physiological range of tissue blood flows, ranging from resting blood flows around 1 mL/minute/g to peak perfusion during maximal vasodilation/hyperemia reaching 4 mL/minute/g in healthy young individuals. The primary clinical application of first-pass perfusion imaging is detecting ischemia in patients with coronary artery disease. An in-plane spatial resolution of at least 2 mm and a temporal resolution one image per heart beat are currently acceptable and typically required for cardiac MR perfusion imaging. To reconcile the opposing needs of higher spatial resolution and adequate temporal updating, k-space undersampling is needed to accelerate image acquisition. Imaging acceleration can take multiple forms, starting with parallel imaging acceleration. Over the last decade, dynamic imaging acceleration has made significant strides forward in the form of combined spatial–temporal acceleration schemes, CS, and most recently, neural networks that effectively learn sparsity structure from training data.

Sequences for cardiac first-pass perfusion imaging can be based on 2D multislice or 3D acquisitions, with the critical difference that, in the latter case, data sampling is only

possible during the relatively quiescent end-systolic pause/diastolic phase of the heart cycle. In the case of 2D multislice imaging, the entire cardiac cycle can be used for image acquisition; however, to freeze cardiac motion, the acquisition of every image must be relatively short compared to the heart cycle (on the order of 100–150 msec or less, depending on the heart rate). As a result of the shorter window for image acquisition with 3D techniques, the requirements for imaging acceleration tend to be considerably higher for 3D compared to 2D perfusion imaging, with acceleration factors of >5 being used with Cartesian k-space sampling schemes,[47] or 2D radial undersampling by similar factors with a stack of stars acquisition. In practice, 2D multislice acquisitions continue to be the prevalent technique used for cardiac perfusion imaging. Most implementations of cardiac first-pass perfusion imaging techniques have settled on using nonslice selective saturation-recovery magnetization preparations before the image readouts to achieve strong T_1-weighting for the depiction of contrast-enhancement in the blood pool and tissue. Alternatively, free-running myocardial perfusion techniques using radial k-space sampling with golden-angle ordering are emerging as alternatives to conventional saturation-prepared perfusion sequences.[48,49] A free-running sequence with the simultaneous multislice acquisition was also developed for whole-heart coverage.[50]

While myocardial tissue enhancement characteristics would appear to be the primary focus for detection of ischemia, quantitative evaluation of myocardial perfusion requires simultaneous measurement of contrast enhancement in the blood pool to determine the so-called arterial input function. Quantitative modeling and analysis of myocardial perfusion generally treat contrast as a blood-borne tracer. Still, image acquisition is based on the indirect detection of contrast through the 1H signal. For the blood pool, this dichotomy means that one needs to correct for the nonlinearity between the measured signal and contrast, since signal enhancement tends to saturate at higher contrast concentrations. The same problem of signal saturation also exists for the myocardial signal, as it is generally thought to be more negligible due to lower net enhancement; however, this may prove to be a misconception for the signal in the vascular space of the tissue at least during initial wash-in of contrast. One of the more noteworthy developments in cardiac perfusion imaging has been the introduction of dual sequences[51] that acquire two image types: 1) myocardial images for all slices with one T_1-weighted contrast setting—determined among other factors by the time delay after saturation preparation—and 2) low-resolution images for one mid-to-basal slice to capture arterial contrast enhancement. These dual sequence techniques are seeing increased usage as interest in quantitative perfusion imaging grows.

For postprocessing applications, machine learning (ML) has been used to relieve the vexing bottleneck of myocardial segmentation. Image segmentation, when performed manually, entails postprocessing times on the order of half an hour or longer per study. Motion correction made in perfusion imaging needs to consider the locally varying contrast enhancement. Methods used for motion correction in perfusion scans include optical flow[52] and robust principal component analysis.[53] The latter provides a way to separate the underlying baseline image from the contrast enhancement for efficient motion correction. For segmentation, convolutional neural networks (eg, with U-Net architecture) have proven to be well suited for automatic segmentation of the myocardial perfusion images,[54] resulting in processing times for automatic segmentation of <1 second for a three-slice perfusion scan.

The culmination of technical advances in myocardial perfusion imaging has taken the form of a sequencing technique that allows adequate multislice coverage of the left ventricle, combined with completely automated postprocessing on the scanner, to produce quantitative perfusion maps of the heart with distribution of myocardial blood flow in units of mL/minute/g. The overall concept for this approach is illustrated in Fig. 4. Automated processing reduces overall processing time from an hour to less than a minute, thereby positioning quantitative perfusion imaging as a technique that can move from the research laboratory to the clinical arena for use in large multicenter studies. Commercially available quantitative myocardial perfusion software packages are also becoming more widely available, facilitating vendor agonist tools.

Hyperpolarized Metabolic Cardiac MR

Clinical cardiac MR primarily targets structural and functional parameters in heart disease. As such, diagnostic information is based mainly on initial myocardial injury assessment or on characterization of impairment as a manifestation of disease progression. However, underlying metabolic changes driving functional adaptations on a cellular level can provide further insight into myocardial injury. Existing metabolic cardiac MR methods are strongly limited by their inherently low sensitivity and metabolic specificity, with motion and prolonged scan durations hampering clinical suitability. Hyperpolarization by dynamic nuclear polarization (DNP), specifically dissolution DNP, is an emerging technology that enables enhancement of spin polarization of endogenous ^{13}C-labeled substrates by >10,000-fold, thereby overcoming the intrinsic sensitivity issues associated with the ^{13}C nucleus[55] (Fig. 5). A labeled substrate is doped with a free-radical, cooled down to 1 K inside a strong magnetic field, and irradiated with microwaves for 1–3 hour, after which the frozen sample is rapidly diluted with a hot buffer. As the polarization of the yielded injectable solution decays with a time constant (T_1) in the order of seconds to minutes, the

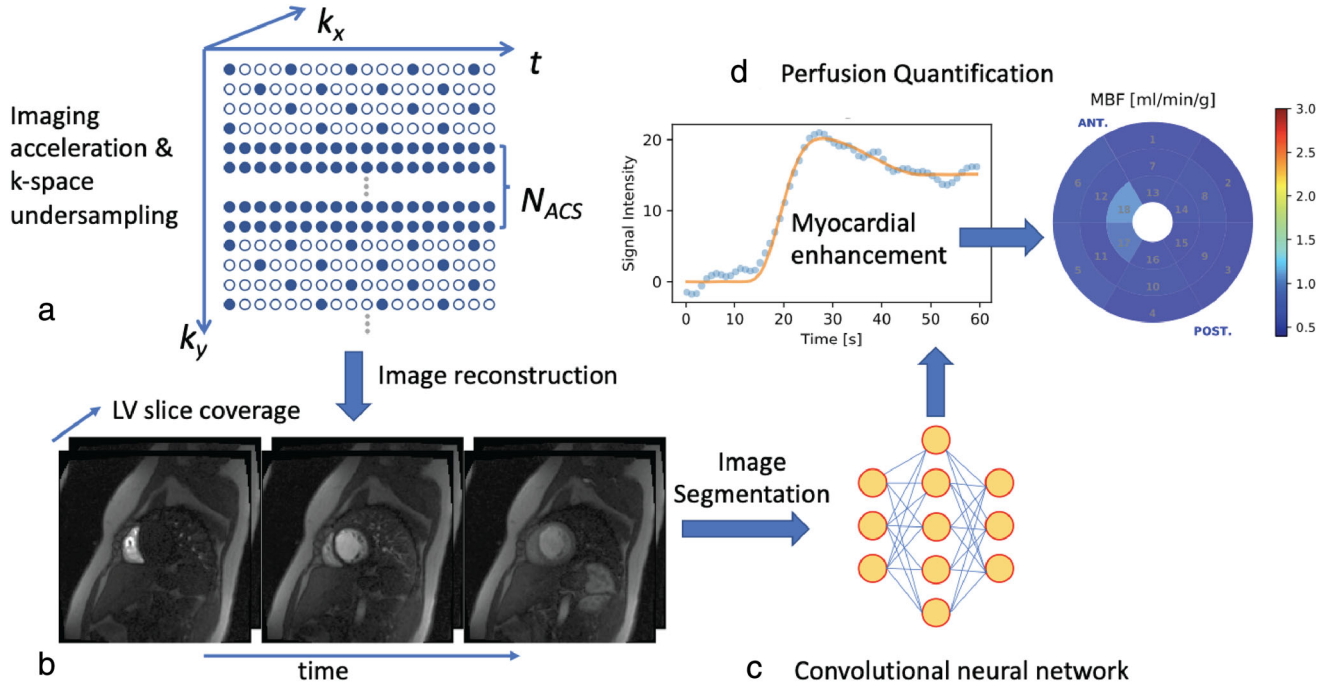

FIGURE 4: Myocardial perfusion: Four key components of quantitative myocardial perfusion imaging include (a) accelerated acquisition during dynamic imaging through k-space undersampling to enable complete coverage of the left ventricle with a temporal resolution equivalent to a heartbeat; (b) image reconstruction and correction for respiratory motion; (c) segmentation of perfusion images using ML and convolutional neural networks; (d) analysis of myocardial contrast enhancement and quantification of myocardial blood flow (MBF) by deconvolution of tissue curves with arterial input or with tracer kinetic model based on segmental or pixel-level signal curves, followed by visualization of results – in this example using a bull's eye display of MBF.

practical window for bolus injection into the patient is usually less than 2 minutes from the time of dissolution. For human administration, rapid quality control protocols prior to injection are the conventional way to ensure patient safety.[56] To date, [1-^{13}C] pyruvate is by far the most widely used molecule in hyperpolarized metabolic imaging, given its favorable physical properties, safety profile, and pivotal role in energy metabolism at the intersection of glycolysis and the tricarboxylic acid (TCA) cycle. It is possible to follow the fate of the ^{13}C label through its downstream enzymatic conversion into [1-^{13}C] lactate, [1-^{13}C] alanine, as well as [^{13}C] bicarbonate, which is reflective of pyruvate dehydrogenase flux (Fig. 6). Under rest conditions, around 70% of the cardiac energy demand is fuelled from fatty acid oxidation; however, relative contribution from glycolysis significantly increases under stress and in various pathologies.[57] While [1-^{13}C] pyruvate probes glycolytic pathways, the label of [2-^{13}C] pyruvate propagates into the TCA cycle, revealing individual steps of energy production. In this context, hyperpolarized cardiac MR provides a series of promising biomarkers for metabolic adaptations in heart disease.

To account for the transient nature of the hyperpolarized signal and the fact that each pulse permanently depletes some of the available signals, novel sequences for hyperpolarized cardiac MR are needed. Most frequently, metabolite images are acquired by selectively exciting each metabolite separately with tailored RF pulses[58] or by reconstruction from an echo-shifted image series.[59] While multislice and even full 3D coverage of the heart have been demonstrated,[60] 2D acquisitions remain the most robust approach. Dynamic imaging, analogous to cardiac perfusion, is often applied to derive markers for the enzymatic activity from the signal time curves. Given the absence of background signals, measured signal intensities are linearly dependent on metabolite concentrations, supporting quantitative analysis. Interpretation of spatial information is often aggravated by geometric distortions stemming from local field inhomogeneities and long readouts, which has led to several correction approaches and improved image accuracy.[61]

The close link between heart failure and altered cardiac metabolism has long been recognized,[57] and has recently been longitudinally investigated with hyperpolarized cardiac MR. Early immuno-metabolic inflammatory processes and reduction in TCA activity[62] were both successfully revealed using hyperpolarized pyruvate. Detection of viable myocardium postinfarction has also recently been demonstrated.[63] Given the apparent link between metabolism and cardiac function, hyperpolarized biomarkers are also being used to better understand how risk factors, such as diabetes mellitus and obesity, contribute to the development of cardiac dysfunction.[64]

Hyperpolarized cardiac MRI is still limited to only a handful of academic centers. Further improvements in image

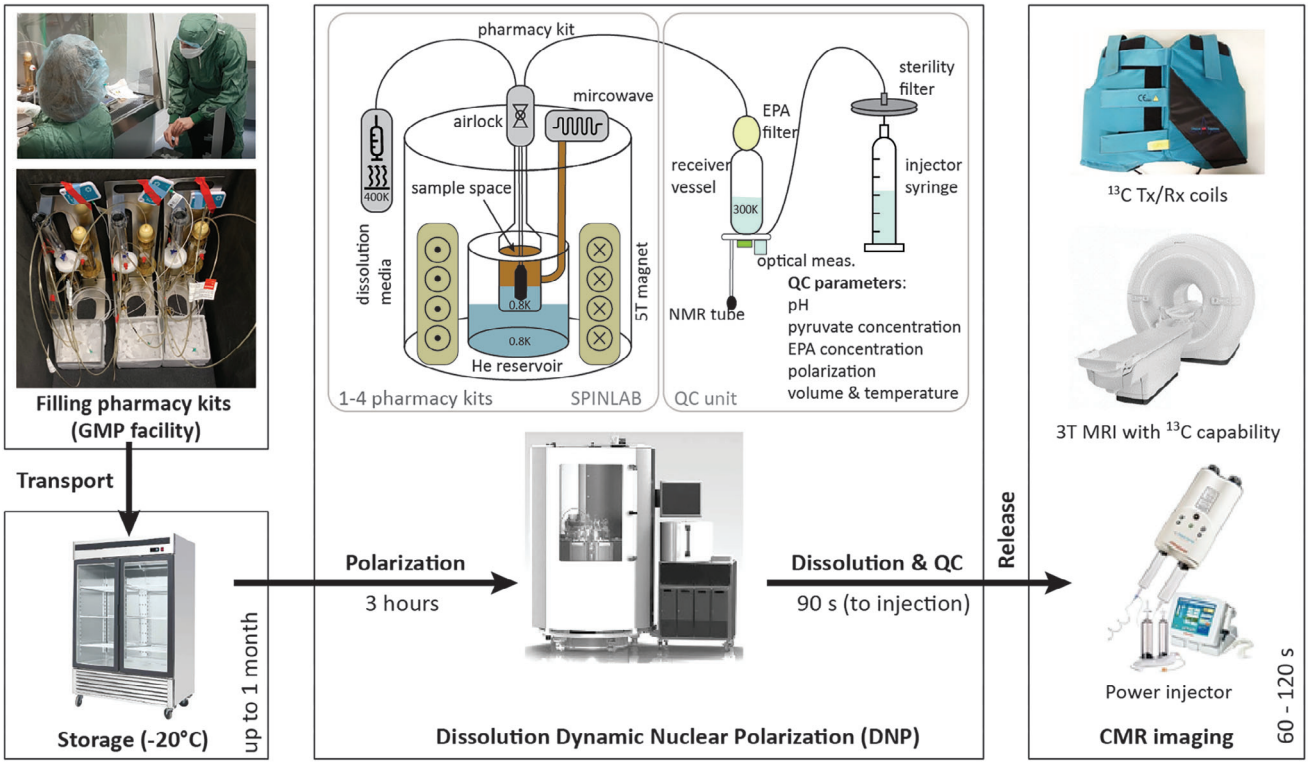

FIGURE 5: Experimental setup for clinical hyperpolarized cardiac MR. ^{13}C labeled pyruvate doped with free radicals (EPA), together with dissolution and neutralization media, is filled into so-called pharmacy kits under sterile GMP conditions. Kits are transported to the clinical site, where they are stored at −20°C until use. For each dose, one kit is thawed, loaded, and polarized at 0.8 K for approx. Upon dissolution, the frozen hyperpolarized pyruvate is dissolved with heated dissolution media (400 K), pH is neutralized in the receiver vessel, and the yield is collected in a power injector syringe. A typical patient dose consists of a 35 mL pyruvate solution at 250 mM concentration, a pH of 6–8, and a temperature of 37°C. A small allocated sample is used to rapidly assess quality control parameters before the syringe is released for administration into the patient. Bolus injection is performed analogously to conventional contrast agents using the same injectors. For hyperpolarized cardiac MR, MR systems need to be equipped with ^{13}C hardware and dedicated transmit and receive coils.

acquisition methodologies and simplified DNP processes are urgently needed to fully exploit its potential. Overcoming technical and operational challenges will enable probing cardiac metabolism to gain insight into cardiovascular disease development and progression.

Exercise Cardiac MR

There has been recent interest in cardiac MR with physiological exercise[65] (Fig. 7). With the availability of a commercial MR-compatible treadmill or supine cycle/stepper ergometer, there have been new reports of cardiac MR's potential clinical application with physiological exercise in different patient populations, including coronary artery disease, valvular disease, athletic heart, congenital heart disease, and heart failure. From a technical imaging perspective, cardiac MR with physiological exercise is very challenging and necessitates highly accelerated imaging. High and rapidly changing heart rates often require real-time imaging with very high temporal resolution. Difficulties in gating, which usually occur right after exercise due to disconnection of ECG leads/artifacts, also pose a significant challenge in robust imaging with exercise.

Accelerated image acquisition techniques such as CS or DL are rapidly enabling imaging during exercise with sufficient spatial and temporal resolution to probe a physiological response to exercise. High-resolution phase-contrast imaging to quantify blood flow in major arteries has also been demonstrated.[66] Free running 2D flow imaging, enabled using radial imaging with DL reconstruction, was recently shown for real-time monitoring of hemodynamic parameters with exercise.[67] The feasibility of four-dimensional (4D) flow MRI for quantification of flow and kinetic energy through major arteries was recently reported.[68] Beyond imaging of flow and cardiac function/volume in response to exercise, myocardial perfusion imaging during exercise could be an alternative to pharmacological exercise with the added benefit of replicating symptoms. A recent pilot study[69] reported the potential role of quantitative imaging with T_1 and T_2 in detecting ischemia with exercise, eliminating the need for pharmacological stress agents and gadolinium contrast. Respiratory motion and rapid heart rate limit the robustness of myocardial perfusion imaging. Emerging techniques for motion correction using slice tracking[70] and free-running myocardial perfusion without ECG gating[71] are promising approaches for more robust

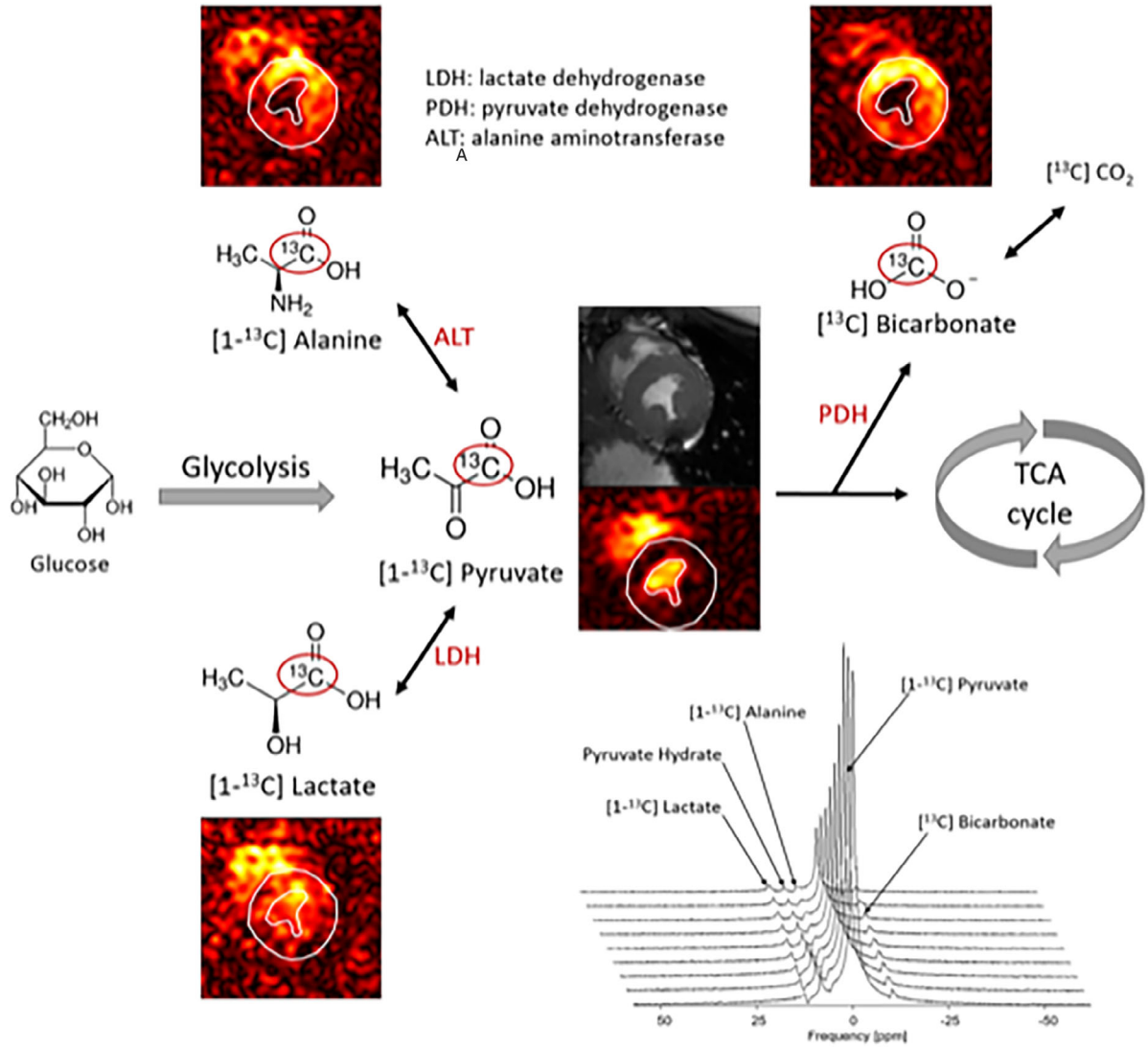

FIGURE 6: Illustration of biomarkers in the glycolytic pathways, enabled by administration of hyperpolarized [1-^{13}C] pyruvate. The ^{13}C label is followed into downstream metabolites, reflecting enzymatic activity and hence metabolic state in the healthy or diseased heart. Both MR spectroscopy and imaging are now being used in clinical studies.

perfusion imaging with exercise. Cardiac MR with exercise is a rapidly growing field of research that requires dedicated technical development to address its unique challenges for powerful imaging. In addition, current exercise equipment is bulky and requires ample space, hindering daily workflow in an MRI suite. There are also significant design improvements that should be considered to reduce exercise equipment size and weight for easier handling. Several research laboratories have developed their own exercise equipment; while this is a worthy endeavor, it is difficult to standardize the exercise protocol. Smaller exercise equipment and a larger magnet bore will ultimately enable more robust patient exercise protocols inside the magnet bore.

Low- Versus High-Field Cardiac MR

While clinical cardiac MR routinely uses 1.5 T and 3 T, there is emerging interest in cardiac MR at both higher and lower magnetic fields. Ultra-high field (>3 T) and low field (<1.5 T) cardiac MR each offer unique clinical applications and have driven the development of new technologies. Cardiac MR at the ultra-high field is motivated by the intrinsically higher SNR and subsequent improvements in spatial and temporal resolution, but is accompanied by high cost and technical challenges. For human imaging, developments in ultra-high-field cardiac MR have primarily used 7 T. The repertoire of cardiac MR methods implemented at 7 T includes cine imaging, 4D flow measurements, dynamic T_2^* mapping, coronary imaging, T_1 mapping,[72–74] and cardiac metabolism by ^{23}Na and ^{31}P imaging.[75,76] Cardiac MR at 7 T presents unique technical challenges. At 7 T, there is considerable residual inhomogeneity in B_0 and B_1^+, even following shimming, and peak B_1^+ is limited by specific absorption rate (SAR). Advanced methods for B_1^+ mapping have been incorporated into cardiac MRI methods at 7 T.[74,77] Transceiver

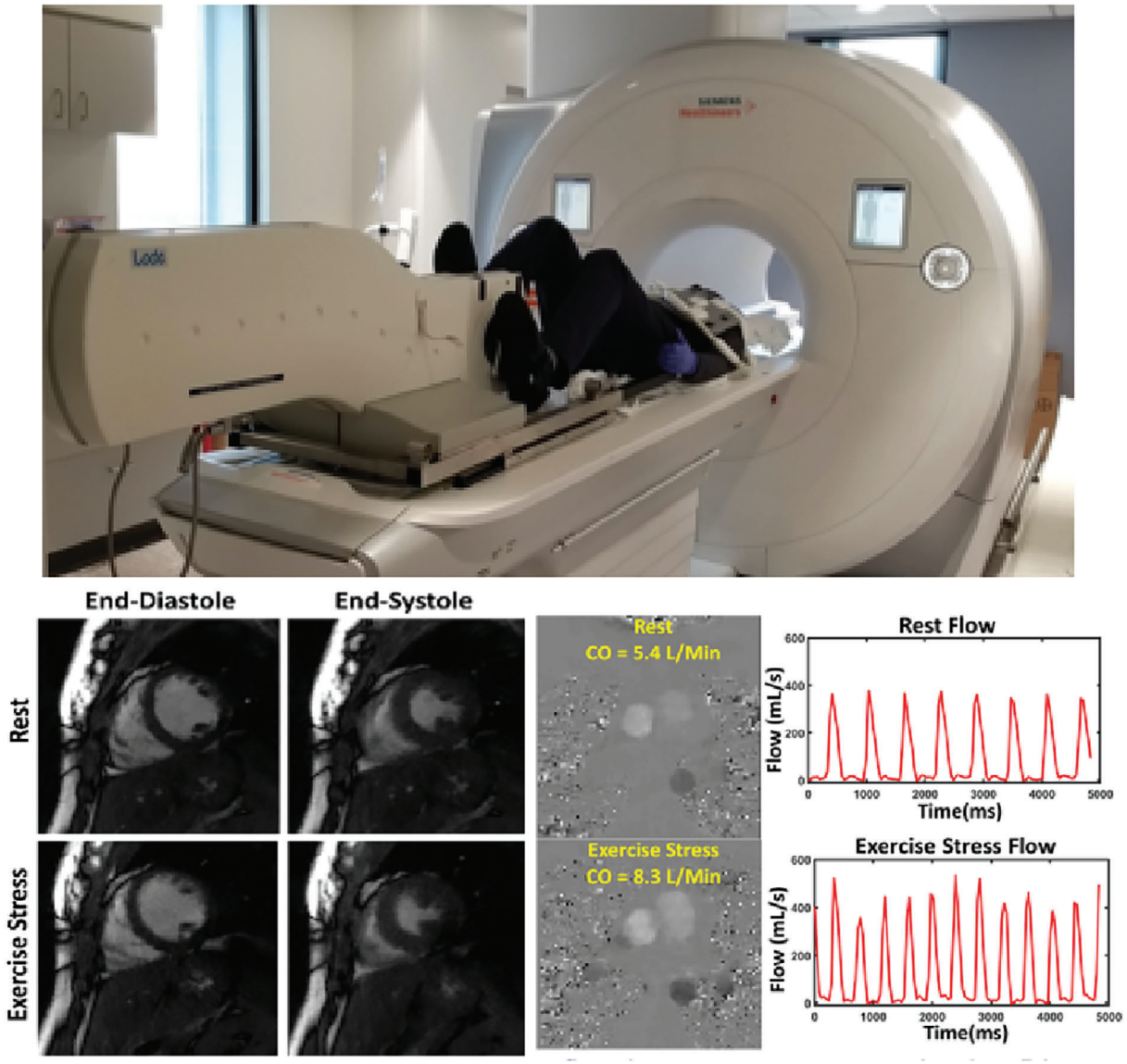

FIGURE 7: Exercise cardiac MR assesses the cardiovascular physiology parameters in response to physiological exercise. Free-breathing highly accelerated imaging (eg, shown with deep learning-based image reconstruction) is necessary for assessment of cardiac function and flow immediately postexercise.

surface coil arrays have also been developed to address B_1^+ inhomogeneity and are routinely applied for patient imaging. High SAR remains an obstacle at 7 T, especially for patients with implanted metallic devices, and further validation of 7 T cardiac MR safety for all patients is required. Finally, acoustic gating[78] or pulse-oximeter gating are utilized to overcome the magnetohydrodynamic effect, which corrupts the ECG signal so that it cannot be used for gating or patient monitoring at 7 T.

Cardiac MR at low fields is primarily motivated by cost-savings, accessibility, patient safety, and ease-of-use, but it is challenged by low SNR. Historically, cardiac MR with commercial low field MRI systems has been difficult due to permanent or resistive magnets and lacking high-performance gradient subsystems or new receiver array technology. However, recent research using modern system designs operating at lower field strengths, such as 0.35 T or 0.55 T, have demonstrated that the technical demands of cardiac MR can be met at lower fields.[79] To assess performance for routine imaging, studies have evaluated cine imaging, phase contrast flow quantification, parametric mapping, and LGE at lower field strengths.[80,81] Moreover, low-field cardiac MR has demonstrated advantages over 1.5 T and 3 T for targeted clinical applications, including combined cardiopulmonary evaluation, MRI-guided catheterization procedures, MRI-guided radio-ablation procedures, and reduced susceptibility artifacts near metallic implants[79] (Fig. 8). Advanced image acquisition and reconstruction methods have an essential role in mitigating SNR loss at the low field without increasing acquisition time. For example, efficient sampling schemes such as EPI

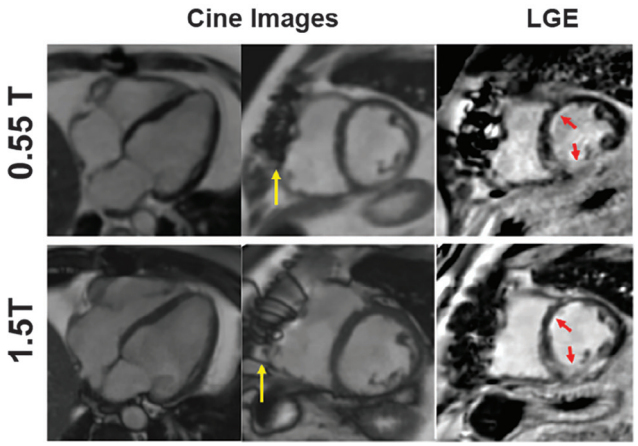

FIGURE 8: Low-field cardiac MR: Comparison of cine imaging and LGE images in a patient with myocardial infarction at 0.55 T and 1.5 T. Cine image quality is comparable between field strengths, and the infarct is visible at both 0.55 T and 1.5 T (red arrows). The susceptibility artifact caused by a sternal wire is reduced to 0.55 T (yellow arrow).

and spiral perform well at lower fields and have been employed for SNR-efficient imaging.[82] Reduced SAR has also allowed flexibility in balanced steady-state free precession (bSSFP) imaging with high flip angles. CS reconstructions have been used to preserve image quality at both 0.35 T and 0.55 T.[80]

The debate of optimal field strength for cardiac MR has been ongoing. Currently, most cardiac MR examinations are still performed at 1.5 T with increasing migration to 3 T imaging. Despite the availability of a 7 T magnetic field over the last decade, there have been only very few cardiac MR studies at this field strength. The pendulum has now swung back to very low field imaging. With recent availability of commercially available 0.55 T MRI systems, we expect healthy growth in cardiac MR at this field strength with some appealing applications such as interventional cardiac MRI or imaging of patients with devices. However, whether we will routinely perform cardiac MR at such a low field remains to be seen.

Accelerating Cardiac MR Acquisition by Deep Learning

Cardiac MR examinations are often longer than other organ MR protocols or alternative imaging modalities. The capacity of cardiac MR to provide information about structure, function, perfusion, tissue characterization, and viability comes at the price of extended scan time. While traditionally, cardiac MR examinations include most sequences as part of a one-stop shop examination, there is a recent trend toward abbreviated cardiac MR examinations. While an abbreviated examination will decrease overall scanning time, individual sequences in a cardiac MR examination could benefit from a shorter scan time by reducing sensitivity to motion or arrhythmia and increasing patient comfort by enabling free-breathing scans. Over the last decades, parallel imaging and CS have been developed to speed up MR acquisition by acquiring less data than needed, enabling 2- to 4-fold acceleration. DL has recently been used to reconstruct artifact-free MR images from highly aliased images or undersampled k-space or interpolate the incomplete k-space data. Lin et al recently provided an overview of the current DL-based technique for MRI reconstruction.[83] In DL, the critical reconstruction parameters are learned from existing datasets and stored in the neural networks during training. The trained DL approaches could be easily used for the reconstruction of new data without the choice of the specific regularization function and hyperparameters as CS. Hauptmann et al[84] proposed a 3D residual U-Net for free-breathing real-time cine with 13-fold acceleration acquired by 2D golden-angle radial bSSFP. More recently, Haji-Valizadeh et al[67] showed that complex-difference DL framework with two 3D U-Nets could accelerate real-time PC-MRI by ~28-fold for rapid free-running real-time assessment of flow hemodynamics. Fast reconstruction of four-dimensional MR angiography of the thoracic aorta has also been recently demonstrated.[85] These preliminary results suggest that DL-based reconstruction is a promising technique in different cardiac MR applications.

Earlier studies employed neural networks (eg, U-Net) to directly remove image artifacts from undersampled data, learn the nonlinear relationship between k-space and image, or interpolate incomplete k-space to full k-space in an end-to-end fashion (Fig. 9A). The end-to-end approach requires a complicated architecture of neural networks and large training datasets to improve robustness and avoid overfitting problems. Subsequently, the physics/model-based unrolling iterative DL reconstructions have been developed.[86] This technique consisted of an end-to-end network for regularization terms and a data consistency layer for data fidelity. It adopted an unrolling iterative algorithm, like the optimization problem in parallel imaging or CS (Fig. 9B). Physics/model-based methods are expected to be trained using smaller training datasets because they are more interpretable.

Most current DL-based cardiac MR reconstruction techniques are based on supervised learning. Large datasets with fully sampled raw data are required, which are not always publicly available. Public datasets would promote research and allow comparison of reconstruction performance among different approaches. Currently, however, publicly available datasets are very limited and often contain healthy subjects and limited clinical indications, impacting generalizability. There is also limited data containing raw coil-by-coil k-space data as these data are not usually stored. While most current cardiac MR reconstruction techniques are based on data collected using Cartesian sampling, non-Cartesian sampling may provide a higher acceleration rate and should be further investigated. Finally, weak-supervised and

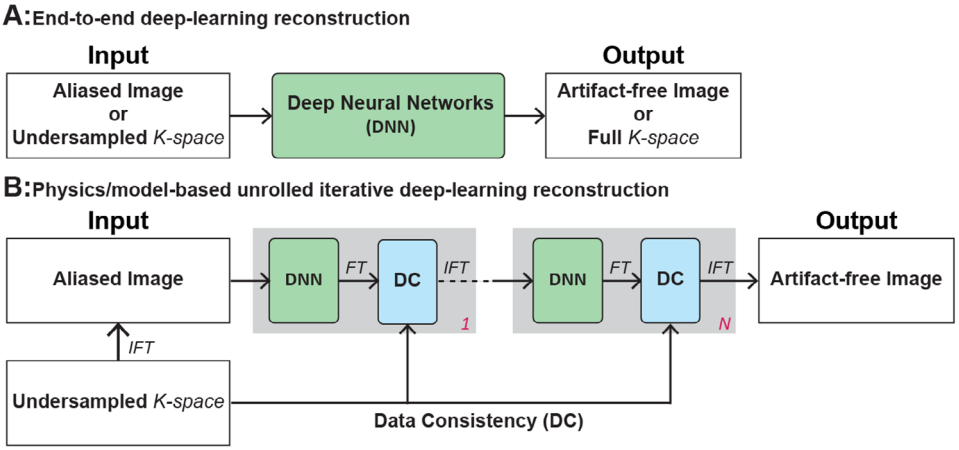

FIGURE 9: Deep learning-based accelerated cardiac MR image reconstruction with end-to-end (a) and physics/model-based unrolled iterative (b). The end-to-end deep-learning approach directly removes the artifact in the aliased image, recovers the undersampled k-space to full, or learns a nonlinear relationship between the aliased subsampled k-space to the artifact-free image. The physics/model-based method cascading several blocks consists of deep neural networks for regularization and data consistency items for data fidelity to simulate an iterative reconstruction process as adopted in paralleling imaging or CS.

unsupervised learning may overcome the lack of large, fully sampled cardiac images.[67]

DL-based cardiac MR acceleration is promising and rapidly evolving. There are still significant gaps in knowledge that should be rigorously studied. Most of the current literature is focused on accelerating cine imaging in healthy subjects, and very little data exist evaluating patients with cardiovascular disease. Furthermore, there is an unmet need to accelerate other cardiac MR sequences such as myocardial perfusion or LGE. There is also limited data available for training DL models for cardiac MR reconstruction, and most available data are from healthy subjects. The robustness of DL-based reconstruction to changes in typical imaging parameters and orientation needs to be fully investigated. The performance of these models in more complicated anatomies, such as patients with congenital heart disease, remains to be evaluated. In summary, further investigation is still necessary to rigorously evaluate DL-based cardiac MR reconstruction for generalizability, diagnostic accuracy, and robustness to different imaging protocol, scan orientation, and vendors.

Automated Cardiac MR Image Analysis With DL

Cardiac MR analysis remains one of the most significant challenges in its clinical adoption. Analysis often involves delineating different anatomical regions and features for calculation of structure, function, flow, or quantification of areas of interest (eg, scar quantification in LGE). Despite the availability of automated approaches for image segmentation in cardiac MR, they are not routinely used, and manual segmentation remains the workhorse in the clinic. With the availability of DL techniques, there is renewed enthusiasm for a fully automated analysis workflow (Fig. 10). The most common application of ML for cardiac MR image analysis is in segmentation of the cardiac chambers or large vascular structures.[87] Due to their initial success, DL-based cine segmentation software is starting to become widely available by commercial vendors. Several DL architectures (eg, 2D/3D convolutional or fully connected neural networks) have been proposed to segment the myocardium. The most established architecture for image segmentation is U-Net,[88] which uses a skip connection between the encoder and decoder to improve segmentation accuracy in a fully connected network.

DL could also be used to facilitate the clinical adoption of myocardial tissue characterization images, an area that has not received enough attention. DL-based techniques have been recently proposed for automating myocardial T_1, T_2, and extra-cellular volume quantification[89,90] and water/fat separation.[91] DL has also been recently used for on-the-fly quality control-driven segmentation of myocardial T_1 mapping.[92] Despite the prognostic value of scar burden, scar quantification in cardiac MR is limited to research studies without standardization, and DL-based scar quantification has shown promise in scar quantification.[93,94] Automated detection of the left ventricle for inline detection of myocardial perfusion has also been recently demonstrated,[95] facilitating future use of cardiac MR perfusion.

Undoubtedly, the immediate impact of DL in cardiac MR will be reducing the burden of image analysis. The rapid and unprecedented adoption of DL-based techniques in cardiac MR image analysis vendors is encouraging. Ongoing and future research will further refine our current techniques and ultimately provide a fully automated workflow wherein images appear with all necessary segmentation and contouring upon loading into the software. The readers' responsibility will thus mostly be quality assessment and result interpretation, rather than the current approach requiring significant efforts focused on contour drawing and subjective evaluation. Such automation will be

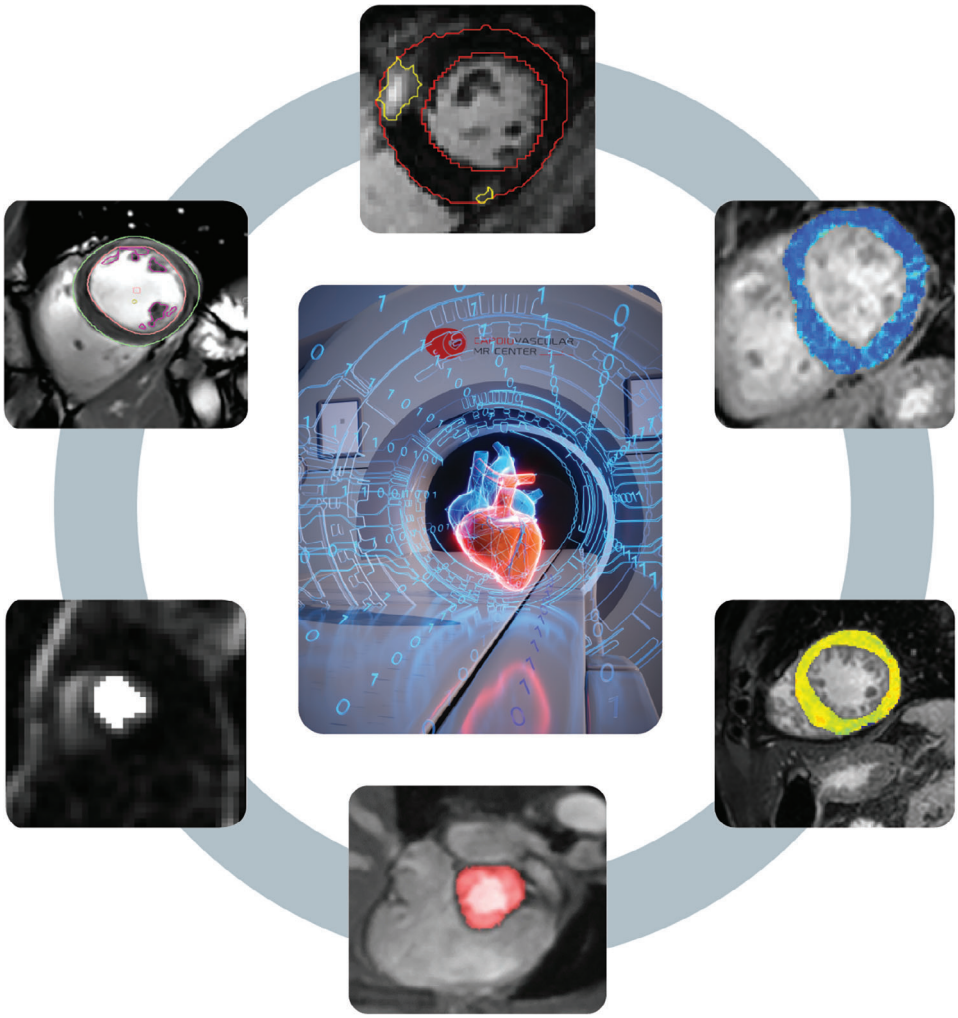

FIGURE 10: Deep learning image segmentation can automate extraction of relevant imaging measurements from different sequences such as cine, flow, perfusion, and tissue mapping. The recent and ongoing advances in deep learning will ultimately enable fully automated analysis, reducing the reader's role to verification of automated-drawn contours, thereby significantly reducing analysis time.

particularly beneficial to sites with little experience in cardiac MR or limited resources for image analysis.

Radiomics Analysis

Radiomics, a novel imaging analysis and interpretation technique, is widely investigated in oncological applications.[96] In radiomics, quantitative features of texture, shape, or histogram are extracted from medical images. Subsequently, radiomic features with diagnostic or prognostic values are extracted using feature selection and used in a prediction/classification model. Figure 11 shows the workflow of radiomic analysis. The first step involves delineation of the region of interest, which often includes the myocardial region. Radiomic features will be extracted from the region of interest. There are several software platforms for the extraction of these markers, with PyRadiomics[97] being the most widely used. Extraction is followed by dimensionality reduction and feature selection. The selected features are then used to build a prediction/diagnostic model. There are numerous models, ranging from an established statistical model to ML-based approaches, that can be used. There is currently no standardized workflow for any of the above steps, resulting in difficulty comparing different studies. There are also differences in the definition of each radiomic feature. Recent efforts have focused on reporting the workflow and detailed descriptions of the definition to improve reproducibility of radiomic studies.

In cardiac MR, radiomics has only recently been applied to myocardial tissue phenotyping. Radiomics analysis of T_1 and T_2 maps revealed an improved diagnosis of acute "infarct-like" myocarditis,[98] as well as acute or chronic heart failure-like myocarditis.[99] The radiomic analysis of T_1 maps enables discrimination between hypertensive heart disease and hypertrophic cardiomyopathy.[100] The radiomics nomogram could also provide incremental information about adverse cardiac events in patients with myocardial infarction.[101] Radiomic features may also provide utility beyond conventional cardiac MR metrics for improved detection

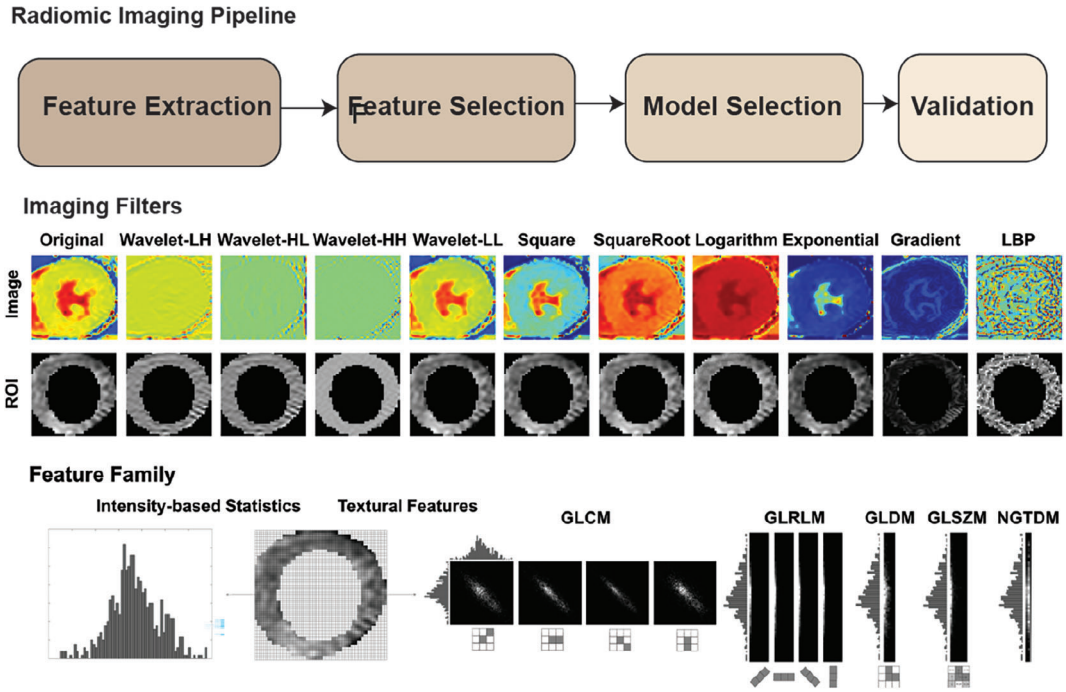

FIGURE 11: Radiomic image analysis of cardiac MR: Radiomic features from regions of interest are extracted from original or transformed regions of interest (eg, myocardium) using different filters. These radiomic features represent different family features such as intensity or textural features. Subsequently, feature and model selection will be performed to identify the features with diagnostic or prognostic values and statistical or machine learning-based models as diagnostic/prediction models. The resulting model should then be evaluated in an independent validation study. The use of external validation datasets collected using different vendors, sites, and so on will provide a meaningful representation of the performance of radiomic analysis.

of the early effects of cardiovascular risk factors on cardiac structure and tissue.[102] Radiomic phenotyping of the myocardium has also been investigated as a marker of fibrosis.[103,104] Despite the promises of radiomic imaging as a novel approach to extract imaging markers with diagnostic and prognostic value beyond standard cardiac MR parameters, there are challenges in the standardization of feature extraction, selection, and model development. Additionally, reproducibility and sensitivity in radiomics remain major research topics, with recent data showing moderate reproducibility,[105,106] sensitivity to imaging sequence parameters,[107] and sensitivity to image acquisition timing in the cardiac cycle.[108] The clinical utility and robustness of radiomic imaging markers should be further investigated using rigorous multicenter and multivendor studies. Also, there is currently no commercially available software that enables radiomic processing of cardiac MR images and integrates all processing steps. Future studies addressing current technical shortcomings of radiomic analysis of cardiac MR and better mechanistic understanding of radiomic features in relation to underlying cardiac pathophysiology will pave the way for future clinical translation and automation of image analysis in cardiac MR.

Future Perspectives

Over the past decade, advances in cardiac MR have made this imaging modality an invaluable test in the management of patients with cardiovascular disease. The growth has been particularly evident in Europe, where cardiac MR is now widely used and included in several clinical guidelines. Recent and ongoing multicenter studies are providing the necessary evidence of the clinical importance of cardiac MR. Recent technical advances in cardiac MR will further advance our field by addressing current shortcomings and obstacles of widespread adoption. Furthermore, development and validation of emerging technologies could provide new insights into cardiovascular pathology. The ongoing two-pronged approach of improving technical capabilities and clinical validation is necessary to better define appropriate use criteria of cardiac MR in daily clinical practice.

Acknowledgments

Dr Weingärtner is supported by NWO Start-Up Grant STU.019.024; 4TU Precision Medicine Program. Campbell-Washburn receives research support from the Division of Intramural Research, National Heart, Lung, and Blood Institute, National Institutes of Health. Dr Nezafat receives grant funding by the NIH 1R01HL129185, 1R01HL129157, 1R01HL127015, and R01HL158098 (Bethesda, MD, USA); and the American Heart Association.

References

1. Kellman P, Arai AE, McVeigh ER, Aletras AH. Phase-sensitive inversion recovery for detecting myocardial infarction using gadolinium-delayed hyperenhancement. Magn Reson Med 2002;47(2):372-383.
2. Basha TA, Tang MC, Tsao C, et al. Improved dark blood late gadolinium enhancement (DB-LGE) imaging using an optimized joint inversion preparation and T2 magnetization preparation. Magn Reson Med 2018;79(1):351-360.
3. Liu CY, Wieben O, Brittain JH, Reeder SB. Improved delayed enhanced myocardial imaging with T2-prep inversion recovery magnetization preparation. J Magn Reson Imaging 2008;28(5):1280-1286.
4. Kim HW, Rehwald WG, Jenista ER, et al. Dark-blood delayed enhancement cardiac magnetic resonance of myocardial infarction. JACC Cardiovasc Imaging 2018;11(12):1758-1769.
5. Fahmy AS, Neisius U, Tsao CW, et al. Gray blood late gadolinium enhancement cardiovascular magnetic resonance for improved detection of myocardial scar. J Cardiovasc Magn Reson 2018;20(1):22.
6. Holtackers RJ, Chiribiri A, Schneider T, Higgins DM, Botnar RM. Dark-blood late gadolinium enhancement without additional magnetization preparation. J Cardiovasc Magn Reson 2017;19(1):64.
7. Basha TA, Akcakaya M, Liew C, et al. Clinical performance of high-resolution late gadolinium enhancement imaging with compressed sensing. J Magn Reson Imaging 2017;46(6):1829-1838.
8. Akcakaya M, Rayatzadeh H, Basha TA, et al. Accelerated late gadolinium enhancement cardiac MR imaging with isotropic spatial resolution using compressed sensing: Initial experience. Radiology 2012;264(3): 691-699.
9. El-Rewaidy H, Neisius U, Mancio J, et al. Deep complex convolutional network for fast reconstruction of 3D late gadolinium enhancement cardiac MRI. NMR Biomed 2020;33(7):e4312.
10. Uhlig J, Al-Bourini O, Salgado R, et al. Gadolinium-based contrast agents for cardiac MRI: Use of linear and macrocyclic agents with associated safety profile from 154 779 European patients. Radiol Cardiothorac Imaging 2020;2(5):e200102.
11. Messroghli DR, Moon JC, Ferreira VM, et al. Clinical recommendations for cardiovascular magnetic resonance mapping of T1, T2, T2* and extracellular volume: A consensus statement by the Society for Cardiovascular Magnetic Resonance (SCMR) endorsed by the European Association for Cardiovascular Imaging (EACVI). J Cardiovasc Magn Reson 2017;19(1):75.
12. Aherne E, Chow K, Carr J. Cardiac T1 mapping: Techniques and applications. J Magn Reson Imaging 2020;51(5):1336-1356.
13. Messroghli DR, Radjenovic A, Kozerke S, Higgins DM, Sivananthan MU, Ridgway JP. Modified look-locker inversion recovery (MOLLI) for high-resolution T1 mapping of the heart. Magn Reson Med 2004;52(1):141-146.
14. Chow K, Flewitt JA, Green JD, Pagano JJ, Friedrich MG, Thompson RB. Saturation recovery single-shot acquisition (SASHA) for myocardial T(1) mapping. Magn Reson Med 2014;71(6):2082-2095.
15. Weingartner S, Akcakaya M, Basha T, et al. Combined saturation/inversion recovery sequences for improved evaluation of scar and diffuse fibrosis in patients with arrhythmia or heart rate variability. Magn Reson Med 2014; 71(3):1024-1034.
16. Roujol S, Weingartner S, Foppa M, et al. Accuracy, precision, and reproducibility of four T1 mapping sequences: A head-to-head comparison of MOLLI, ShMOLLI, SASHA, and SAPPHIRE. Radiology 2014; 272(3):683-689.
17. Triadyaksa P, Oudkerk M, Sijens PE. Cardiac T2* mapping: Techniques and clinical applications. J Magn Reson Imaging 2020;52(5): 1340-1351.
18. Kellman P, Xue H, Spottiswoode BS, et al. Free-breathing T2* mapping using respiratory motion corrected averaging. J Cardiovasc Magn Reson 2015;17(1):3.
19. Huang TY, Liu YJ, Stemmer A, Poncelet BP. T2 measurement of the human myocardium using a T2-prepared transient-state TrueFISP sequence. Magn Reson Med 2007;57(5):960-966.
20. Giri S, Chung YC, Merchant A, et al. T2 quantification for improved detection of myocardial edema. J Cardiovasc Magn Reson 2009;11 (1):56.
21. Ding H, Fernandez-de-Manuel L, Schar M, et al. Three-dimensional whole-heart T2 mapping at 3T. Magn Reson Med 2015;74(3):803-816.
22. Akcakaya M, Basha TA, Weingartner S, Roujol S, Berg S, Nezafat R. Improved quantitative myocardial T2 mapping: Impact of the fitting model. Magn Reson Med 2015;74(1):93-105.
23. Sprinkart AM, Luetkens JA, Traber F, et al. Gradient spin echo (GraSE) imaging for fast myocardial T2 mapping. J Cardiovasc Magn Reson 2015;17(1):12.
24. van Heeswijk RB, Feliciano H, Bongard C, et al. Free-breathing 3 T magnetic resonance T2-mapping of the heart. JACC Cardiovasc Imaging 2012;5(12):1231-1239.
25. Bustin A, Hua A, Milotta G, et al. High-spatial-resolution 3D whole-heart MRI T2 mapping for assessment of myocarditis. Radiology 2021; 298(3):578-586.
26. Basha TA, Bellm S, Roujol S, Kato S, Nezafat R. Free-breathing slice-interleaved myocardial T2 mapping with slice-selective T2 magnetization preparation. Magn Reson Med 2016;76(2):555-565.
27. Blume U, Lockie T, Stehning C, et al. Interleaved T1 and T2 relaxation time mapping for cardiac applications. J Magn Reson Imaging 2009; 29(2):480-487.
28. Kvernby S, Warntjes M, Engvall J, Carlhall CJ, Ebbers T. Clinical feasibility of 3D-QALAS—single breath-hold 3D myocardial T1- and T2-mapping. Magn Reson Imaging 2017;38:13-20.
29. Akcakaya M, Weingartner S, Basha TA, Roujol S, Bellm S, Nezafat R. Joint myocardial T1 and T2 mapping using a combination of saturation recovery and T2 -preparation. Magn Reson Med 2016;76(3): 888-896.
30. Guo R, Cai X, Kucukseymen S, et al. Free-breathing simultaneous myocardial T1 and T2 mapping with whole left ventricle coverage. Magn Reson Med 2021;85(3):1308-1321.
31. Liu Y, Hamilton J, Rajagopalan S, Seiberlich N. Cardiac magnetic resonance fingerprinting: Technical overview and initial results. JACC Cardiovasc Imaging 2018;11(12):1837-1853.
32. Christodoulou AG, Shaw JL, Nguyen C, et al. Magnetic resonance multitasking for motion-resolved quantitative cardiovascular imaging. Nat Biomed Eng 2018;2(4):215-226.
33. Musthafa HS, Dragneva G, Lottonen L, et al. Longitudinal rotating frame relaxation time measurements in infarcted mouse myocardium in vivo. Magn Reson Med 2013;69(5):1389-1395.
34. Zhou Z, Nguyen C, Chen Y, et al. Optimized CEST cardiovascular magnetic resonance for assessment of metabolic activity in the heart. J Cardiovasc Magn Reson 2017;19(1):95.
35. Stoeck CT, Scott AD, Ferreira PF, et al. Motion-induced signal loss in in vivo cardiac diffusion-weighted imaging. J Magn Reson Imaging 2020;51(1):319-320.
36. Edelman RR, Gaa J, Wedeen VJ, et al. In vivo measurement of water diffusion in the human heart. Magn Reson Med 1994;32(3):423-428.
37. Nguyen C, Fan Z, Sharif B, et al. In vivo three-dimensional high resolution cardiac diffusion-weighted MRI: A motion compensated diffusion-prepared balanced steady-state free precession approach. Magn Reson Med 2014;72(5):1257-1267.
38. Stoeck CT, von Deuster C, Genet M, Atkinson D, Kozerke S. Second-order motion-compensated spin echo diffusion tensor imaging of the human heart. Magn Reson Med 2016;75(4):1669-1676.
39. Lasic S, Szczepankiewicz F, Dall'Armellina E, et al. Motion-compensated b-tensor encoding for in vivo cardiac diffusion-weighted imaging. NMR Biomed 2020;33(2):e4213.

40. Teh I, McClymont D, Zdora MC, et al. Validation of diffusion tensor MRI measurements of cardiac microstructure with structure tensor synchrotron radiation imaging. J Cardiovasc Magn Reson 2017;19(1):31.

41. Khalique Z, Ferreira PF, Scott AD, et al. Diffusion tensor cardiovascular magnetic resonance of microstructural recovery in dilated cardiomyopathy. JACC Cardiovasc Imaging 2018;11(10):1548-1550.

42. Gotschy A, von Deuster C, Weber L, et al. CMR diffusion tensor imaging provides novel imaging markers of adverse myocardial remodeling in aortic stenosis. JACC Cardiovasc Imaging 2021;14(7):1472-1474.

43. Rodriguez EK, Hunter WC, Royce MJ, Leppo MK, Douglas AS, Weisman HF. A method to reconstruct myocardial sarcomere lengths and orientations at transmural sites in beating canine hearts. Am J Physiol 1992;263(1 Pt 2):H293-H306.

44. Perotti LE, Verzhbinsky IA, Moulin K, et al. Estimating cardiomyofiber strain in vivo by solving a computational model. Med Image Anal 2021;68:101932.

45. Moulin K, Croisille P, Viallon M, Verzhbinsky IA, Perotti LE, Ennis DB. Myofiber strain in healthy humans using DENSE and cDTI. Magn Reson Med 2021;86(1):277-292.

46. Spinner GR, Stoeck CT, Mathez L, von Deuster C, Federau C, Kozerke S. On probing intravoxel incoherent motion in the heart-spin-echo versus stimulated-echo DWI. Magn Reson Med 2019;82(3):1150-1163.

47. Manka R, Wissmann L, Gebker R, et al. Multicenter evaluation of dynamic three-dimensional magnetic resonance myocardial perfusion imaging for the detection of coronary artery disease defined by fractional flow reserve. Circ Cardiovasc Imaging 2015;8:(5):e003061.

48. DiBella EV, Chen L, Schabel MC, Adluru G, McGann CJ. Myocardial perfusion acquisition without magnetization preparation or gating. Magn Reson Med 2012;67(3):609-613.

49. Sharif B, Dharmakumar R, Arsanjani R, et al. Non-ECG-gated myocardial perfusion MRI using continuous magnetization-driven radial sampling. Magn Reson Med 2014;72(6):1620-1628.

50. Tian Y, Mendes J, Wilson B, et al. Whole-heart, ungated, free-breathing, cardiac-phase-resolved myocardial perfusion MRI by using Continuous Radial Interleaved simultaneous Multi-slice acquisitions at sPoiled steady-state (CRIMP). Magn Reson Med 2020;84(6):3071-3087.

51. Gatehouse P, Lyne J, Smith G, Pennell D, Firmin D. T2* effects in the dual-sequence method for high-dose first-pass myocardial perfusion. J Magn Reson Imaging 2006;24(5):1168-1171.

52. Benovoy M, Jacobs M, Cheriet F, Dahdah N, Arai AE, Hsu LY. Robust universal nonrigid motion correction framework for first-pass cardiac MR perfusion imaging. J Magn Reson Imaging 2017;46(4):1060-1072.

53. Scannell CM, Villa ADM, Lee J, Breeuwer M, Chiribiri A. Robust nonrigid motion compensation of free-breathing myocardial perfusion MRI data. IEEE Trans Med Imaging 2019;38(8):1812-1820.

54. Xue H, Davies RH, Brown LAE, et al. Automated inline analysis of myocardial perfusion MRI with deep learning. Radiol Artif Intell 2020;2(6):e200009.

55. Ardenkjaer-Larsen JH, Fridlund B, Gram A, et al. Increase in signal-to-noise ratio of >10,000 times in liquid-state NMR. Proc Natl Acad Sci USA 2003;100(18):10158-10163.

56. Ardenkjaer-Larsen JH, Leach AM, Clarke N, Urbahn J, Anderson D, Skloss TW. Dynamic nuclear polarization polarizer for sterile use intent. NMR Biomed 2011;24(8):927-932.

57. Stanley WC, Recchia FA, Lopaschuk GD. Myocardial substrate metabolism in the normal and failing heart. Physiol Rev 2005;85(3):1093-1129.

58. Larson PE, Kerr AB, Chen AP, et al. Multiband excitation pulses for hyperpolarized 13C dynamic chemical-shift imaging. J Magn Reson 2008;194(1):121-127.

59. Sigfridsson A, Weiss K, Wissmann L, et al. Hybrid multiband excitation multiecho acquisition for hyperpolarized (13)C spectroscopic imaging. Magn Reson Med 2015;73(5):1713-1717.

60. Gordon JW, Hansen RB, Shin PJ, Feng Y, Vigneron DB, Larson PEZ. 3D hyperpolarized C-13 EPI with calibrationless parallel imaging. J Magn Reson 2018;289:92-99.

61. Geraghty BJ, Lau JYC, Chen AP, Cunningham CH. Dual-echo EPI sequence for integrated distortion correction in 3D time-resolved hyperpolarized (13)C MRI. Magn Reson Med 2018;79(2):643-653.

62. Dodd MS, Atherton HJ, Carr CA, et al. Impaired in vivo mitochondrial Krebs cycle activity after myocardial infarction assessed using hyperpolarized magnetic resonance spectroscopy. Circ Cardiovasc Imaging 2014;7(6):895-904.

63. Apps A, Lau JYC, Miller J, et al. Proof-of-principle demonstration of direct metabolic imaging following myocardial infarction using hyperpolarized 13C CMR. JACC Cardiovasc Imaging 2021;14(6):1285-1288.

64. Rider OJ, Apps A, Miller J, et al. Noninvasive in vivo assessment of cardiac metabolism in the healthy and diabetic human heart using hyperpolarized (13)C MRI. Circ Res 2020;126(6):725-736.

65. Craven TP, Tsao CW, La Gerche A, Simonetti OP, Greenwood JP. Exercise cardiovascular magnetic resonance: Development, current utility and future applications. J Cardiovasc Magn Reson 2020;22(1):65.

66. Weber TF, von Tengg-Kobligk H, Kopp-Schneider A, Ley-Zaporozhan J, Kauczor HU, Ley S. High-resolution phase-contrast MRI of aortic and pulmonary blood flow during rest and physical exercise using a MRI compatible bicycle ergometer. Eur J Radiol 2011;80(1):103-108.

67. Haji-Valizadeh H, Guo R, Kucukseymen S, et al. Highly accelerated free-breathing real-time phase contrast cardiovascular MRI via complex-difference deep learning. Magn Reson Med 2021;86(2):804-819.

68. Macdonald JA, Beshish AG, Corrado PA, et al. Feasibility of cardiovascular four-dimensional flow MRI during exercise in healthy participants. Radiol Cardiothorac Imaging 2020;2(3):e190033.

69. Nakamori S, Fahmy A, Jang J, et al. Changes in myocardial native T1 and T2 after exercise stress: A noncontrast CMR pilot study. JACC Cardiovasc Imaging 2020;13(3):667-680.

70. Pflugi S, Roujol S, Akcakaya M, et al. Accelerated cardiac MR stress perfusion with radial sampling after physical exercise with an MR-compatible supine bicycle ergometer. Magn Reson Med 2015;74(2):384-395.

71. Haji-Valizadeh H, Guo R, Kucukseymen S, et al. Artifact reduction in free-breathing, free-running myocardial perfusion imaging with interleaved non-selective RF excitations. Magn Reson Med 2021;86(2):954-963.

72. Hess AT, Bissell MM, Ntusi NA, et al. Aortic 4D flow: Quantification of signal-to-noise ratio as a function of field strength and contrast enhancement for 1.5T, 3T, and 7T. Magn Reson Med 2015;73(5):1864-1871.

73. van Elderen SG, Versluis MJ, Westenberg JJ, et al. Right coronary MR angiography at 7 T: A direct quantitative and qualitative comparison with 3 T in young healthy volunteers. Radiology 2010;257(1):254-259.

74. Rodgers CT, Piechnik SK, Delabarre LJ, et al. Inversion recovery at 7 T in the human myocardium: Measurement of T(1), inversion efficiency and B(1) (+). Magn Reson Med 2013;70(4):1038-1046.

75. Rodgers CT, Clarke WT, Snyder C, Vaughan JT, Neubauer S, Robson MD. Human cardiac 31P magnetic resonance spectroscopy at 7 Tesla. Magn Reson Med 2014;72(2):304-315.

76. Stoll VM, Clarke WT, Levelt E, et al. Dilated cardiomyopathy: Phosphorus 31 MR spectroscopy at 7 T. Radiology 2016;281(2):409-417.

77. Clarke WT, Robson MD, Rodgers CT. Bloch-Siegert B1+-mapping for human cardiac (31) P-MRS at 7 tesla. Magn Reson Med 2016;76(4):1047-1058.

78. Frauenrath T, Hezel F, Renz W, et al. Acoustic cardiac triggering: A practical solution for synchronization and gating of cardiovascular magnetic resonance at 7 Tesla. J Cardiovasc Magn Reson 2010;12:67.

79. Campbell-Washburn AE, Ramasawmy R, Restivo MC, et al. Opportunities in interventional and diagnostic imaging by using high-performance low-field-strength MRI. Radiology 2019;293(2):384–393.

80. Bandettini WP, Shanbhag SM, Mancini C, et al. A comparison of cine CMR imaging at 0.55 T and 1.5 T. J Cardiovasc Magn Reson 2020;22 (1):37.

81. Varghese J, Craft J, Crabtree CD, et al. Assessment of cardiac function, blood flow and myocardial tissue relaxation parameters at 0.35 T. NMR Biomed 2020;33(7):e4317

82. Restivo MC, Ramasawmy R, Bandettini WP, Herzka DA, Campbell-Washburn AE. Efficient spiral in-out and EPI balanced steady-state free precession cine imaging using a high-performance 0.55T MRI. Magn Reson Med 2020;84(5):2364-2375.

83. Lin DJ, Johnson PM, Knoll F, Lui YW. Artificial intelligence for MR image reconstruction: An overview for clinicians. J Magn Reson Imaging 2021;53(4):1015-1028.

84. Hauptmann A, Arridge S, Lucka F, Muthurangu V, Steeden JA. Real-time cardiovascular MR with spatio-temporal artifact suppression using deep learning-proof of concept in congenital heart disease. Magn Reson Med 2019;81(2):1143-1156.

85. Haji-Valizadeh H, Shen D, Avery RJ, et al. Rapid reconstruction of four-dimensional MR angiography of the thoracic aorta using a convolutional neural network. Radiol Cardiothorac Imaging 2020;2(3): e190205.

86. Schlemper J, Caballero J, Hajnal JV, Price AN, Rueckert D. A deep cascade of convolutional neural networks for dynamic MR image reconstruction. IEEE Trans Med Imaging 2018;37(2):491-503.

87. Tao Q, Yan W, Wang Y, et al. Deep learning-based method for fully automatic quantification of left ventricle function from cine MR images: A multivendor, multicenter study. Radiology 2019;290(1): 81-88.

88. Ronneberger O, Fischer P, Brox T. U-Net: Convolutional networks for biomedical image segmentation. In: Navab N, Hornegger J, Wells WM, Frangi AF, editors. *Medical image computing and computer-assisted intervention – MICCAI 2015*, Vol 9351. Cham: Springer International Publishing; 2015. p 234-241.

89. Zhu Y, Fahmy AS, Duan C, Nakamori S, Nezafat R. Automated myocardial T2 and extracellular volume quantification in cardiac MRI using transfer learning-based myocardium segmentation. Radiol Artif Intell 2020;2(1):e190034.

90. Fahmy AS, El-Rewaidy H, Nezafat M, Nakamori S, Nezafat R. Automated analysis of cardiovascular magnetic resonance myocardial native T1 mapping images using fully convolutional neural networks. J Cardiovasc Magn Reson 2019;21(1):7.

91. Goldfarb JW, Craft J, Cao JJ. Water-fat separation and parameter mapping in cardiac MRI via deep learning with a convolutional neural network. J Magn Reson Imaging 2019;50(2):655-665.

92. Hann E, Popescu IA, Zhang Q, et al. Deep neural network ensemble for on-the-fly quality control-driven segmentation of cardiac MRI T1 mapping. Med Image Anal 2021;71:102029.

93. Fahmy AS, Neisius U, Chan RH, et al. Three-dimensional deep convolutional neural networks for automated myocardial scar quantification in hypertrophic cardiomyopathy: A multicenter multivendor study. Radiology 2020;294(1):52-60.

94. Fahmy AS, Rowin EJ, Chan RH, Manning WJ, Maron MS, Nezafat R. Improved quantification of myocardium scar in late gadolinium enhancement images: Deep learning based image fusion approach. J Magn Reson Imaging 2021;54(1):303-312.

95. Xue H, Tseng E, Knott KD, et al. Automated detection of left ventricle in arterial input function images for inline perfusion mapping using deep learning: A study of 15,000 patients. Magn Reson Med 2020;84 (5):2788-2800.

96. Gillies RJ, Kinahan PE, Hricak H. Radiomics: Images are more than pictures, they are data. Radiology 2016;278(2):563-577.

97. van Griethuysen JJM, Fedorov A, Parmar C, et al. Computational radiomics system to decode the radiographic phenotype. Cancer Res 2017;77(21):e104-e107.

98. Baessler B, Luecke C, Lurz J, et al. Cardiac MRI texture analysis of T1 and T2 maps in patients with infarctlike acute myocarditis. Radiology 2018;289(2):357-365.

99. Baessler B, Luecke C, Lurz J, et al. Cardiac MRI and texture analysis of myocardial T1 and T2 maps in myocarditis with acute versus chronic symptoms of heart failure. Radiology 2019;292(3):608-617.

100. Neisius U, El-Rewaidy H, Nakamori S, Rodriguez J, Manning WJ, Nezafat R. Radiomic analysis of myocardial native T1 imaging discriminates between hypertensive heart disease and hypertrophic cardiomyopathy. JACC Cardiovasc Imaging 2019;12(10):1946-1954.

101. Ma Q, Ma Y, Wang X, et al. A radiomic nomogram for prediction of major adverse cardiac events in ST-segment elevation myocardial infarction. Eur Radiol 2021;31(2):1140-1150.

102. Cetin I, Raisi-Estabragh Z, Petersen SE, et al. Radiomics signatures of cardiovascular risk factors in cardiac MRI: Results from the UK biobank. Front Cardiovasc Med 2020;7:591368.

103. Baessler B, Mannil M, Maintz D, Alkadhi H, Manka R. Texture analysis and machine learning of non-contrast T1-weighted MR images in patients with hypertrophic cardiomyopathy—Preliminary results. Eur J Radiol 2018;102:61-67.

104. Neisius U, El-Rewaidy H, Kucukseymen S, et al. Texture signatures of native myocardial T1 as novel imaging markers for identification of hypertrophic cardiomyopathy patients without scar. J Magn Reson Imaging 2020;52(3):906-919.

105. Jang J, Ngo LH, Mancio J, et al. Reproducibility of segmentation-based myocardial radiomic features with cardiac MRI. Radiol Cardiothorac Imaging 2020;2(3):e190216.

106. Baessler B, Weiss K, Pinto Dos Santos D. Robustness and reproducibility of radiomics in magnetic resonance imaging: A phantom study. Invest Radiol 2019;54(4):221-228.

107. Jang J, El-Rewaidy H, Ngo LH, et al. Sensitivity of myocardial radiomic features to imaging parameters in cardiac MR imaging. J Magn Reson Imaging 2021.

108. Alis D, Yergin M, Asmakutlu O, Topel C, Karaarslan E. The influence of cardiac motion on radiomics features: Radiomics features of non-enhanced CMR cine images greatly vary through the cardiac cycle. Eur Radiol 2021;31(5):2706-2715.